Tunability of reflection and transmission spectra of two periodically corrugated metallic plates, obtained by control of the interactions between plasmonic and photonic modes

Avner Yanai and Uriel Levy*

Department of Applied Physics, The Benin School of Engineering and Computer Science, The Hebrew University of Jerusalem, Jerusalem 91904, Israel
**Corresponding author: ulevy@cc.huji.ac.il*

Received April 21, 2010; accepted June 8, 2010;
posted June 10, 2010 (Doc. ID 127113); published July 9, 2010

We theoretically study the interactions between plasmonic and photonic modes within a structure that is composed of two thin corrugated metallic plates, embedded in air. We show that the interactions depend on the symmetry of the interacting modes. This observation is explained by the phase difference between the Fourier components of the two gratings. The phase can be controlled by laterally shifting one grating with respect to the other. Therefore, this relative shift provides an efficient "knob" that allows one to control the interaction between the various modes, resulting in an efficient modulation of light transmission and reflection in the proposed structure. Based on this concept we show that the investigated structure can be used as a tunable plasmonic filter.

OCIS codes: 240.0240, 240.6680, 050.0050, 310.2790.

1. INTRODUCTION

The field of surface plasmon polaritons (SPPs) [1] has been rapidly developing over the past couple of decades. One of the active plasmonic-related research topics is the waveguiding characteristics of multilayered plasmonic structures [2]. A basic example for such a structure is that of a thin metal film sandwiched between two dielectric (insulating) media [insulator/metal/insulator (IMI)]. For a thin enough film, the SPP modes guided by the two dielectric-metal interfaces are coupled through the metal, thus creating supermodes that exhibit a dispersion varying with the metal thickness. A variant of the IMI structure that has been studied recently is a doubly corrugated metallic layer which was analyzed for sinusoidal [3,4] and rectangular [5,6] gratings, with possible applications for a bandgap plasmonic laser and optical filters. A more complex multilayered configuration is the double metal plate structure, comprising an insulator/metal/insulator/metal/insulator (IMIMI) interface. The dispersion equations and the waveguiding characteristics of this configuration have been studied by [7–9]. This structure was recently applied for the calculation of the optical forces between the metallic plates [10]. In this paper, we study a symmetric one-dimensional IMIMI structure, of which each of the two metallic layers is periodically corrugated. We analyze this configuration and show that the relative shift between the corrugated interfaces controls the interaction between the modes supported by the structure. Furthermore, we demonstrate that the control of these interactions enables tunable filtering properties of both the reflection and the transmission spectra. The computer simulations used for this study are based on the rigorous coupled wave analysis (RCWA) method, also known as the Fourier modal method. We apply the factorization rules that lead to faster convergence for transverse magnetic (TM) polarization [11–14]. The paper is structured as follows. In Section 2, the modes supported by the structure are described and classified into groups. In Section 3, it is demonstrated how the interactions between the plasmonic and the photonic modes form an effective "absorption gap," both under normal and oblique incidences. In Section 4, we show how the shift in absorbance lines can be utilized to obtain tunable filtering properties of the reflection and transmission spectra. Furthermore, we show (to our knowledge, for the first time) how the poor transmission can be enhanced by introducing a large refractive index contrast between the substrate/superstrate and the air gap separating the metallic plates.

2. MODES OF AN IMIMI STRUCTURE

Figure 1(a) shows a flat double plate structure, with metal layer thickness H_M and dielectric gap between the plates, H_A. As previously analyzed [7–10], a symmetric double metal plate supports four plasmonic modes. These modes can be classified as two long-range surface plasmon polariton (LRSPP) modes, which can be either symmetric or antisymmetric with respect to each other (defined as LRS and LRA), and two short-range surface plasmon polariton (SRSPP) modes, which can also be either symmetric or antisymmetric with respect to each other (SRS and SRA).

Throughout this paper the plane of symmetry is assumed to be in the middle of the dielectric gap H_A ($z=0$)

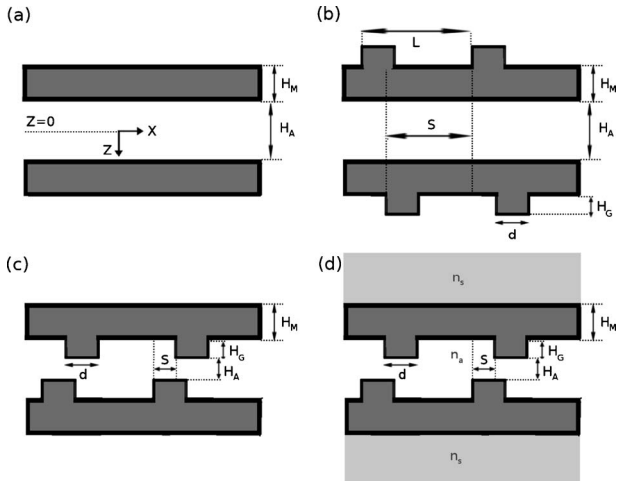

Fig. 1. Schematic drawing of an IMIMI structure. (a) Flat interfaces. (b) Outward grating modulation. (c) Inward grating modulation. (d) Non-homogeneous dielectric environment with inward grating modulation.

and the symmetry is defined with regard to the magnetic field H_y. The characteristic equation for the symmetric plasmonic modes in a symmetric IMIMI structure embedded in uniform dielectric media is given by

$$\tanh\left(\frac{k_D H_A}{2}\right) = -\frac{\frac{k_D k_M}{\varepsilon_D \varepsilon_M} + \left(\frac{k_M}{\varepsilon_M}\right)^2 \tanh(k_M H_M)}{\frac{k_D k_M}{\varepsilon_D \varepsilon_M} + \left(\frac{k_D}{\varepsilon_D}\right)^2 \tanh(k_M H_M)}, \quad (1)$$

where $k_i^2 = k_X^2 - \varepsilon_i k_0^2$ is the decay constant along the Z direction and $i = M, D$ for the metallic and dielectric layers, respectively. To obtain the antisymmetric modes, the term $\tanh(k_D H_A/2)$ should be replaced with $\coth(k_D H_A/2)$. Besides these four modes, the structure also supports Fabry–Perot modes (FPMs) with $k_x = 0$ that reside between the two metal plates. Also, guided modes exist within the dielectric gap between the plates. For a not too thin metallic layer thickness, these modes can be approximately regarded as the TM metallic slab waveguide. As will be shown, the FPM and the TM guided modes have an important role when considering potential applications of the investigated structure.

Next we add a rectangular grating modulation with grating depth of H_G [either outward or inward; see Figs. 1(b) and 1(c)]. Thus, the permittivity function takes the form $\varepsilon(x) = \sum_{h=-\infty}^{\infty} \varepsilon_h \exp(j2\pi hx/L)$, where L is the grating period. The Fourier components of the permittivity function in the grating region are given by [11]

$$\varepsilon_h = [(\varepsilon_M - \varepsilon_D)\sin(\pi h d/L)/(\pi h)]\exp(-j2\pi hS/L), \quad (2)$$

where d/L is the duty cycle of the metallic ridge and S is the relative shift between the two gratings. Under normally incident illumination, the allowed k-vectors of the modes take discrete values of the multiples of the grating vector K ($K = 2\pi/L$).

3. MODE COUPLING AND INTERACTION

A one-dimensional periodic structure has a bandgap which resides at the edges of the Brillouin zone. It was shown that for a periodic structure with grating vector $1K$, no bandgaps are formed at normal incidence ($k_X = 0$), unless the grating has an additional $2K$ Fourier component [3]. As can be observed from Eq. (2), for the specific case of $d/L = 0.5$, the even Fourier terms vanish and thus no $2K$ components exist. Therefore, for such a case no bandgaps should be formed at normal incidence. This issue and its consequences will be addressed again in Section 4. When considering a double plate structure in which each of the plates is modulated by a grating [Figs. 1(b) and 1(c)], an additional "gap" mechanism arises. This gap is due to mode coupling as a result of phase matching between two distinct modes. The phase matching is highly dependent on the mode symmetry as will be shown immediately. This mode coupling mechanism can be explained by the coupled mode theory [15,16] and is well known in photonic structures [17,18]. It was also observed in an adiabatically varying plasmonic structure [19] and by the interaction between a waveguide mode (WGM) and a plasmonic mode [20].

A. Weak Interaction between Symmetric and Antisymmetric Modes

To demonstrate the above, we investigated a double plate structure of the type shown in Fig. 1(b) with the parameters $H_G = 80$ nm, $H_M = 30$ nm, $L = 1000$ nm, and $d/L = 0.75$. The materials are assumed to be air and Ag, i.e., $\varepsilon_D = 1$ and ε_M is defined by the Drude model $\varepsilon(\omega) = \varepsilon_\infty - (\varepsilon_0 - \varepsilon_\infty)\omega_P^2/(\omega^2 + i\omega\gamma)$ with the following parameters: $\varepsilon_\infty = 4.017$, $\varepsilon_0 = 4.896$, $\omega_P = 1.419 \times 10^{16}$ rad/s, and $\gamma = 1.117 \times 10^{14}$ rad/s. In Fig. 2, the calculated absorption of this structure under normally incident TM plane wave illumination is plotted for three different values of S/L as a function of the incident wavelength and the separation distance H_A. The absorption (Ab) is calculated by the

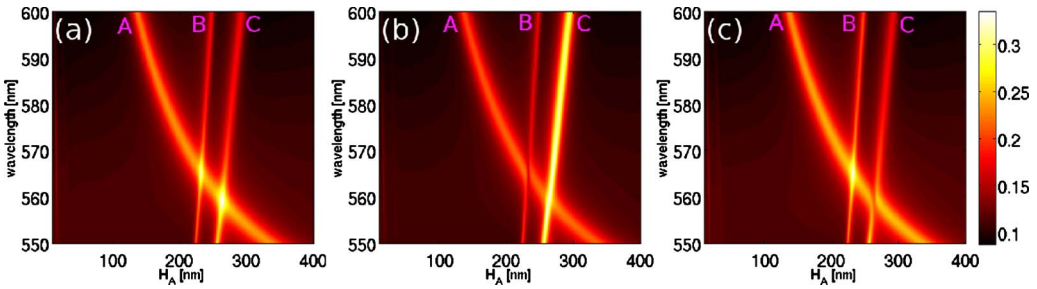

Fig. 2. (Color online) Absorption as a function of the incident wavelength and H_A for three different relative shifts between the metal plates for the case of outward pointing gratings as shown in Fig. 1(b). (a) $S/L = 0$, (b) $S/L = 0.25$, (c) $S/L = 0.5$.

RCWA algorithm using the relation $Ab=1-T-R$, where T and R are the total transmission and reflection diffraction efficiencies, respectively. In the absence of absorption, $T+R=1$. Three different modes can be observed, designated as A, B, and C. Mode A is the SRS mode. Mode B is the first order FPM and is therefore antisymmetric with regard to the magnetic field inside the air gap between the plates. Mode C is an antisymmetric guided mode. This mode is not a solution of the characteristic equations of the non-modulated IMIMI structure [Eq. (1)] and can be approximated as the slab TM_1 mode. The condition for exciting this mode is $L=m\lambda_0/n_{\text{eff}}$ where m is an integer and n_{eff} is the effective index of the mode, which is smaller than the one for the wavelengths calculated in Fig. 2. Thus wavelengths smaller than the period of the grating (1 μm) excite this mode. Figure 3 shows the magnetic field distribution of the three modes, calculated for a vacuum wavelength of 600 nm. It can be seen that the SRS mode has an effective wavelength of $L/2$ [Fig. 3(a)], whereas the FPM [Fig. 3(b)] is invariant along the x-axis, indicating the absence of a k_X component. The SRS mode can be identified by solving Eq. (1) for the symmetric case and by observing the symmetric magnetic fields that are strongly localized near the metallic plates as shown in Fig. 3(a). Figure 3(c) shows that the effective wavelength of the TM_1 slab mode occupies a single unit cell indicating that the effective index is smaller than 1 (the unit cell is larger than the vacuum wavelength). The TM_1 can be identified by solving the ordinary TM waveguide characteristic equation.

To conclude, all three modes have different k_X-vectors: for mode A, $k_X=2K$; for mode B, $k_X=0K$; and for mode C, $k_X=1K$. In all three insets of Fig. 2 mode A intersects with modes B and C. However, the intersections result in different interactions in the three considered cases. In Fig. 2(a) there is no interaction between the different modes, and the absorption at the intersection of the A–B and A–C modes is simply the summation of the absorption of the two relevant modes. Moreover, the modes do not alter their characteristics at the intersection region or in its surrounding. In Fig. 2(b), one can observe an interaction between the modes, in the form of mode coupling at the A–B intersection. This results in an anti-crossing between modes A and B. The A–C intersection is kept unchanged, i.e., no interaction between these two modes is observed. Figure 2(c) shows the opposite scenario, where the A–B modes are not interacting whereas anti-crossing is observed around the A–C intersection.

Let us now describe the mechanism that is affecting the interaction between the modes. Due to the fact that mode A is symmetric with $k_X=2K$ while mode B is antisymmetric with $k_X=0K$, the phase matching that allows the $A\leftrightarrow B$ transition to occur involves interaction with the $2K$ grating component (more generally, other interactions, e.g., $0K_{\text{FPM}}+2K_{\text{SRS}}=3K-1K$ might be possible as well, but are weaker than the "straightforward" $0K_{\text{FPM}}+2K_{\text{SRS}}=2K$ interaction and are therefore not considered). In Table 1, the values of the phase Φ [$\Phi(hK)$ is the phase of the hth Fourier component, as calculated from Eq. (2)] are summarized for the three different values of S/L that were considered in Fig. 2. First, we consider the $A\leftrightarrow B$ transition. As modes A and B are of opposite symmetry, no interaction is possible unless they undergo a relative phase shift of π with respect to the mirror plane $z=0$. This is similar to the condition for coupling of symmetric and antisymmetric modes in photonic grating couplers (see, e.g., [18]). For $S/L=0$, this condition cannot be satisfied. In this case the gratings have no phase difference with respect to each other and therefore the necessary π phase shift cannot be provided. However, for $S/L=0.25$, $\Phi(2K)$ undergoes a π phase shift. This explains the anti-crossing in Fig. 2(b). For $S/L=0.5$, $\Phi(2K)$ has again the same phase as for $S/L=0$. Therefore, no anti-crossing is seen in Fig. 2(c). For the $A\leftrightarrow C$ transition, the considerations are similar, only now the interaction is provided by the $1K$ component. Again, for $S/L=0$, no interaction is possible, as the A and C modes have opposite symmetry. As shown in Table 1, the interacting grating component (i.e., $1K$) undergoes a π phase shift for $S/L=0.5$. Therefore, for these modes we see an anti-crossing in Fig. 2(c). In Fig. 2(b), only a partial phase match (phase difference of $\pi/2$) is obtained for the $A\leftrightarrow C$ transition, and no clear anti-crossing can be observed.

B. Strong Interaction between Modes of the Same Symmetry

When the gratings are pointing "outward" (with regard to the dielectric region between the two metal plates) as in the previously described case, the anti-crossings observed in Fig. 2 are generally weak. This is because the interactions between the modes occur mostly in the dielectric region between the plates, while the gratings are placed in the opposite sides of the metal plates. Now we consider the case where the gratings are pointing inward as shown in Fig. 1(c). The structural parameters are identical to the

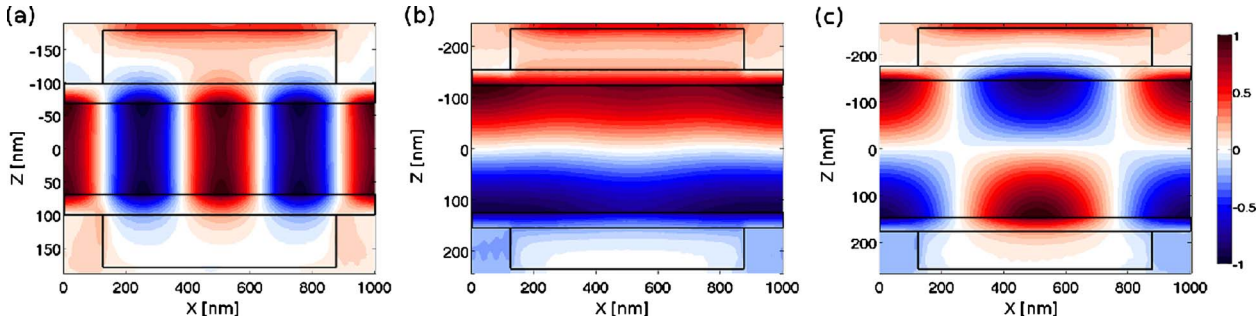

Fig. 3. (Color online) Normalized real part of the magnetic field distribution (H_y) calculated at $\lambda=600$ nm and $S/L=0$ for (a) SRS mode ($H_A=137.5$ nm), (b) FPM ($H_A=248.5$ nm), (c) TM_1 mode ($H_A=293$ nm). The square rectangles define the boundaries of the metallic grating ridges and the metallic plates.

Table 1. Phases of the Three Modes and Phase Matching between the Different Modes for Three Values of Relative Grating Shift

S/L	$\Phi(0K)$	$\Phi(1K)$	$\Phi(2K)$	$A\leftrightarrow B$ $(2K\leftrightarrow 0K)$	$A\leftrightarrow C$ $(2K\leftrightarrow 1K)$
0	0	0	0	No PM[a]	No PM
0.25	0	$\pi/2$	π	PM	Partial PM
0.5	0	π	0	No PM	PM

[a]PM stands for phase matching.

previously discussed structure (Subsection 3.A) except that $H_G=30$ nm, with the gratings extending into the dielectric gap between the plates. The absorption curves of this structure are plotted in Figs. 4(a)–4(c), for three different values of S/L. Figure 4(d) shows schematically the curves of the original unperturbed modes as they would approximately exist without inter-modal interaction, superimposed on the $S/L=0$ case [also shown in Fig. 4(a)]. These unperturbed modes are marked by the green (designated as A_A and A_S), blue (B_A and B_S), and white (C_A and C_S) lines. As in the previous simpler case, we have three modes A, B, and C which are the SRSPP modes, FPM, and WGMs, respectively, where the subscripts denote the symmetry. In this example we are considering a larger domain both in wavelength and in separation between the plates. As a result, we can now observe both symmetries of the three modes. In Fig. 4(d), A_A and A_S represent the SRA and SRS modes, respectively. As expected, these two modes can be seen to have the same characteristics in the limit of $H_A\rightarrow\infty$ as the two IMI modes have no interaction. B_A and B_S are the first and second order FPMs, respectively, having opposite symmetry. C_A and C_S are WGMs (TM_1 and TM_2, respectively). As before, the K-vectors of the SRSPP, FPM, and WGM are $2K$, $0K$, and $1K$, respectively. In Fig. 4(a), we can observe the interactions $A_A\leftrightarrow B_A$, $A_S\leftrightarrow B_S$, and $A_A\leftrightarrow C_A$ as expected since only interactions between modes of the same symmetry are allowed. The $A_S\leftrightarrow C_S$ interaction cannot be observed. The absence of this transition may be explained by the strong $A_S\leftrightarrow B_S$ transition, masking other interactions. In Fig. 4(b) the $2K$ interactions of opposite symmetry are allowed. Therefore we see the $A_S\leftrightarrow B_A$ and $A_A\leftrightarrow B_S$ interactions. We also identify interactions involving the $1K$ component between modes of the same symmetry, because the $1K$ component is partially matched [i.e., $A_A\leftrightarrow C_A$ and also $A_S\leftrightarrow C_S$ which in contrary to Fig. 4(a) is now visible as it is not masked by the $A_S\leftrightarrow B_S$ interaction which is now forbidden]. In Fig. 4(c) we see interactions between modes of opposite symmetry due to the $1K$ component ($A_S\leftrightarrow C_A$ and $A_A\leftrightarrow C_S$) and continue to see interactions between modes of the same symmetry that are due to the $2K$ component ($A_A\leftrightarrow B_A$ and $A_S\leftrightarrow B_S$).

C. Mode Hybridization Under Oblique Incidence

We now consider the effect of changing the angle of incidence. For small oblique incident angles (incident TM plane wave is tilted in the X-Z plane), the above discussed plasmonic modes will have two possible frequencies which solve the SPP characteristic equation [Eq. (1)] for a given

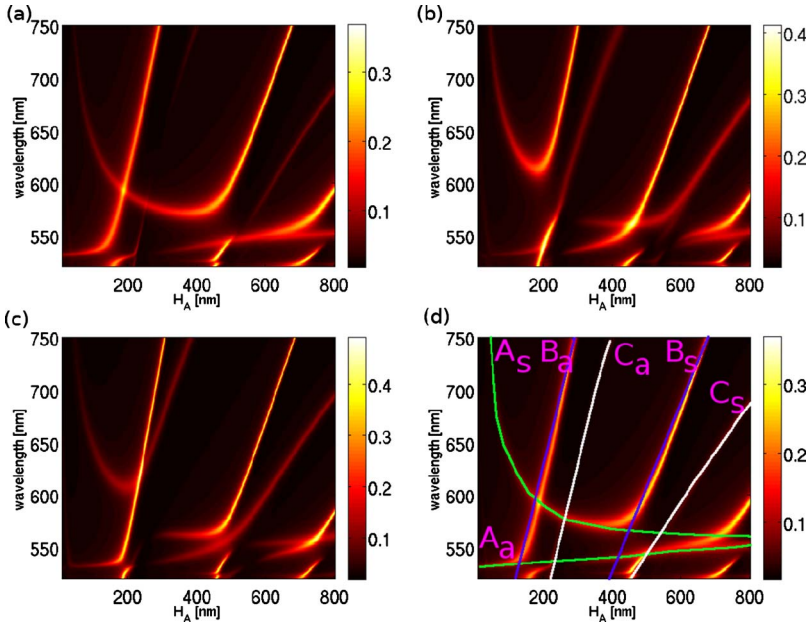

Fig. 4. (Color online) Absorption as a function of the incident wavelength and H_A for three different relative shifts between the metal plates for the case of inward pointing gratings as shown in Fig. 1(c). (a) $S/L=0$, (b) $S/L=0.25$, (c) $S/L=0.5$. (d) Schematic drawing of the supported modes as they would approximately appear with no inter-modal interaction. The schematic curves are superimposed on the $S/L=0$ scenario that is also shown in Fig. 3(a). The green, blue, and white lines represent SRSPP modes, FPM, and WGM, respectively (both symmetric and antisymmetric).

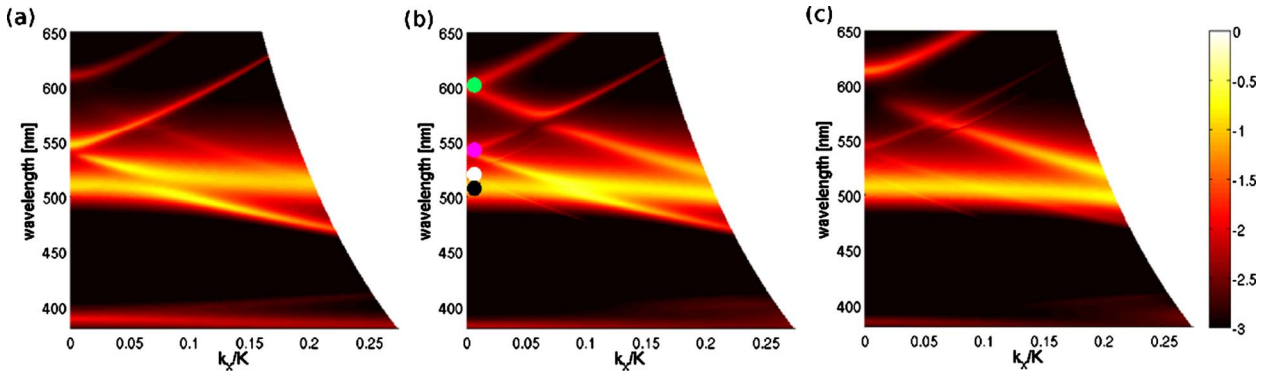

Fig. 5. (Color online) Logarithmic scaled plot of the absorption as function of the incident wavelength and the normalized transverse wavevector k_X/K for the following three relative shifts: (a) $S/L=0$, (b) $S/L=0.25$. The SRS, SRA, LRS, and FPM are designated at $k_X=0$ (from top to bottom) with green, purple, white, and black dots, respectively. (c) $S/L=0.5$.

k_X. Thus, two branches of the SPP modes originating from $k_X=0$ appear at a dispersion diagram of the structure. This is in contrast to the FPM mode which still exhibits a single branch, because the FPM condition for k_Z is uniquely satisfied by an increase in the frequency with the increase in the incident angle. As a consequence of the existence of two separate SPP branches, distinct plasmonic modes now intersect at $k_X\neq 0$ and may interact with each other. In Fig. 5, a dispersion diagram is plotted for the "inward" grating structure with the parameters $H_A=190$ nm, $H_M=30$ nm, $H_G=10$ nm, $L=500$ nm, and $d/L=0.75$, for three different relative shifts. Now the grating period is halved compared with the previous case and thus the SPP modes have a $1K$ wavevector and there is no coupling to the WGM (the $1K$ component for $L=1000$ nm is equivalent to a non-existing $0.5K$ component for $L=500$ nm). From Figs. 5(a) and 5(c) one can clearly observe the appearance of a bandgap at $k_X=0$ for $S/L=0$ and $S/L=0.5$. This bandgap is due to the $2K$ grating component, as explained in [3,6]. As explained in these references, for $S/L=0.25$, the bandgaps disappear. In Fig. 5(b) (where there are no gaps at $k_X=0$), we have marked the excited modes as SRS, SRA, LRS, and FPM. The additional LRA mode is very poorly coupled in this specific configuration and is therefore not observed (we have observed that, for thicker gratings, coupling to the LRA becomes significant).

To help put the current discussion in the context of the previous section, we also plotted the absorption of the same structure for normally incident light as a function of H_A (see Fig. 6). The data set at $H_A=190$ nm (see vertical dashed lines in Fig. 6) corresponds to the $k_x=0$ case in Fig. 5. Next we discuss the interactions between the modes.

1. Interactions between Plasmonic and Photonic Modes

The SRA and FPM interact for $S/L=0$ around $k_X/K=0.075$ since both modes have the same symmetry. Because the interaction between the FPM and SPP modes is now obtained through the $1K$ component, we see that for $S/L=0.5$ the FPM and SRS are interacting. Both interactions can be also observed for $S/L=0.25$. Yet, the interaction strength is weaker, because the phase matching is partial.

2. Interactions between the Plasmonic Modes

The mechanism of interactions between plasmonic modes at a single layer for $k_X\neq 0$ was analyzed in [6,21] and found to originate from the $2K$ component. Therefore, we expect that interaction between distinct plasmonic modes will occur if the $2K$ component will provide the required phase shift to match the symmetry between the plasmonic modes. Thus, in our configuration, interactions between symmetric and antisymmetric modes should be possible only for the case of $S/L=0.25$. Indeed, it is seen that for such a shift the SRA and SRS modes are interacting, whereas for $S/L=0$ and $S/L=0.5$ no interaction between these modes can be observed. These interactions are observed as anti-crossings near $k_X/K=0.06$ in Fig. 5(b). The interaction between the LRS and SRS is expected to show an opposite behavior. This is because both

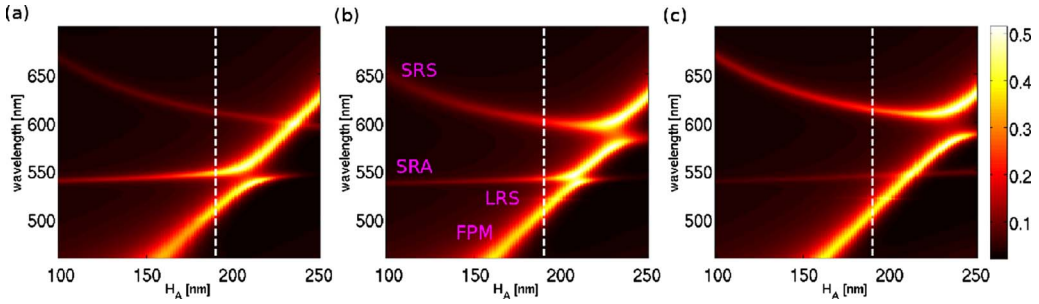

Fig. 6. (Color online) The absorption as function of the incident wavelength and the plate separation under normally incident light for the same structure as in Fig. 5. The white dashed line corresponds to the case of $H_A=190$ nm at $k_X=0$ plotted in Fig. 5. Three relative shifts were considered: (a) $S/L=0$, (b) $S/L=0.25$, (c) $S/L=0.5$.

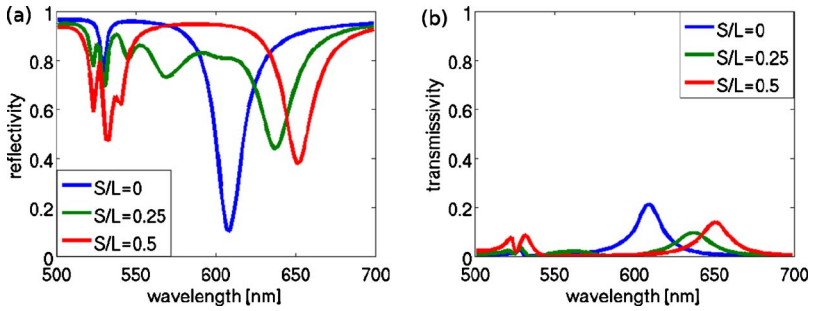

Fig. 7. (Color online) (a) Reflectivity and (b) transmissivity as functions of the incident wavelength.

modes have the same symmetry and therefore the $2K$ component must not provide any phase shift. Indeed, interactions are observed for $S/L=0$ and $S/L=0.5$ but not for $S/L=0.25$.

4. TUNABLE FILTERING OBTAINED BY SHIFTING THE RELATIVE GRATING POSITION

One of the potential applications of the investigated structure is a tunable filter, where tuning can be obtained by controlling the relative shift between the two plates. Such a tunable filter has been previously proposed for multilayered dielectric structures [22–24]. Tunable filtering can be obtained for both the transmission and reflection spectra of the structure. However, while the reflection is significant, the transmission is low. We will first consider the case of reflection tunability, and then discuss the modifications needed for obtaining high transmission that is needed for an efficient tunable transmission filter.

Let us consider a structure with the following parameters: $L=500$ nm, $H_G=30$ nm, and $H_M=30$ nm. We choose $d/L=0.5$ to maximize the coupling to the SPP modes. As only the $1K$ component is interacting, the cases of $S/L=0$ and $S/L=0.5$ are the two extreme cases (maximal phase difference of π for the $1K$ component between these two cases). In Fig. 7 the reflection and the transmission as functions of wavelength are plotted for three values of the relative shift, $S/L=0$, $S/L=0.25$, and $S/L=0.5$, with a separation of $H_A=196$ nm. For $S/L=0$ the first order FPM and the SRS do not interact, providing a low reflection coefficient of $R=0.1$ at their crossing point. For $S/L=0.5$ the modes interact and the reflection increases to $R=0.9$ at the same wavelength. In addition, one can notice that the resonance dip in reflection is shifted in wavelength. For example, Fig. 7(a) shows a shift of the reflection dip from 608 to ~650 nm. These effects can be used for the realization of a tunable plasmonic filter.

While similar shifts in the wavelength of resonance are also observed for the transmission of light through the investigated structure [Fig. 7(b)], the overall transmission efficiency is seen to be very low. As shown before [25,26], the transmission mechanism is via localized SPP modes that reside in the grating ridges, and not through the flat surface SPPs [27]. Therefore, in order to enhance the transmission, it is desirable to confine more energy in the grating ridges, at the expense of a lower energy concentration at the flat surfaces. A possible way to achieve this is by changing the substrate and superstrate refractive indices to $n_S=2.6$ [e.g., by using a silicon carbide substrate; see Fig. 1(d) for a schematic of the structure]. By keeping the metal layers thin (~20 nm) the SPPs on both interfaces remain coupled. The SPPs tend to be more confined in the lower-index dielectric interface and to be more radiating at the higher-index dielectric. Thereby, for an inward grating configuration, more energy is confined at the grating ridges that reside near the lower-index material (Fig. 8). In Fig. 8 the transmission and reflection spectra are plotted for the following configuration: $H_A=25$ nm, $H_M=25$ nm, and $H_G=40$ nm. The substrate and the superstrate have a dielectric index of $n_S=2.6$ and the plates are separated by an air gap ($n_a=1$). It is observed that the transmission efficiency is greatly enhanced. The structure still obtains mirror symmetry around $Z=0$; however the plasmonic modes can no longer be identified as LRSPP or SRSPP as these only exist for the cases for which each plate is embedded in a homogeneous dielectric medium. Still, because of the mirror symmetry, the modes can be classified as symmetric and antisymmetric modes of the overall structure. It can be seen for the absorption spectra in Fig. 8(c) that an anti-crossing is formed for $S/L=0.5$. This anti-crossing generates the observed shift

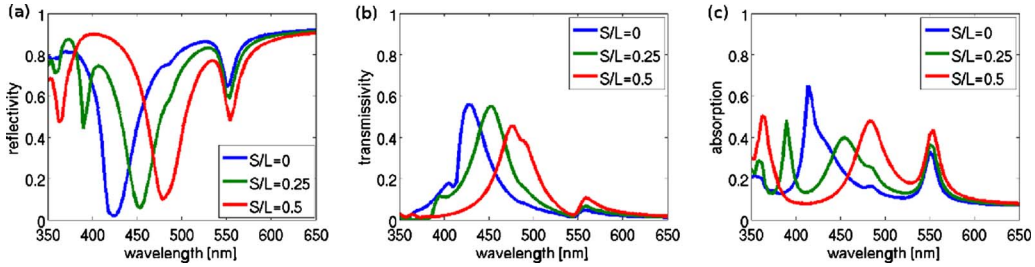

Fig. 8. (Color online) (a) Reflectivity, (b) transmissivity, and (c) absorption as functions of the incident wavelength, for the double plate embedded in an inhomogeneous dielectric index configuration.

in the reflection and transmission peaks seen in Figs. 8(a) and 8(b), respectively.

5. CONCLUSIONS

We study the plasmonic and photonic modes that are supported by an IMIMI structure made of thin metallic layers. It is shown that by adding grating modulation to both metallic layers, the supported modes can interact. This interaction is explained by the symmetry of the modes and the relative phase shift provided by the grating Fourier components. The various interactions are explored both under normally and oblique incident illuminations. Finally, we show that a relative lateral shift between the two gratings provides tunable filtering properties. Because of the diversity of the supported modes and their interactions, this structure seems to be of interest for further research and for investigating additional applications, e.g., the selective excitation of plasmonic modes for plasmonic focusing applications [28,29], and the design of guided-mode resonant filters [30].

ACKNOWLEDGMENTS

The authors acknowledge the support of the Israeli Science Foundation (ISF), the Israeli Ministry of Science, and the Peter Brojde Center for Innovative Engineering and Computer Science.

REFERENCES

1. W. L. Barnes, A. Dereux, and T. W. Ebbesen, "Surface plasmon subwavelength optics," Nature **424**, 824–830 (2003).
2. S. A. Maier, *Plasmonics: Fundamentals and Applications* (Springer, 2007).
3. W. L. Barnes, T. W. Preist, S. C. Kitson, and J. R. Sambles, "Physical origin of photonic energy gaps in the propagation of surface plasmons on gratings," Phys. Rev. B **54**, 6227–6244 (1996).
4. R. Hooper and J. R. Sambles, "Coupled surface plasmon polaritons on thin metal slabs corrugated on both surfaces," Phys. Rev. B **70**, 045421 (2004).
5. D. Gérard, L. Salomon, F. de Fornel, and A. Zayats, "Analysis of the Bloch mode spectra of surface polaritonic crystals in the weak and strong coupling regimes: grating-enhanced transmission at oblique incidence and suppression of SPP radiative losses," Opt. Express **12**, 3652–3663 (2004).
6. T. Okamoto, J. Simonen, and S. Kawata, "Plasmonic band gaps of structured metallic thin films evaluated for a surface plasmon laser using the coupled-wave approach," Phys. Rev. B **77**, 115425 (2008).
7. G. I. Stegeman and J. J. Burke, "Long-range surface-plasmons in electrode structures," Appl. Phys. Lett. **43**, 221–223 (1983).
8. R. Zia, M. Selker, P. Catrysse, and M. Brongersma, "Geometries and materials for subwavelength surface plasmon modes," J. Opt. Soc. Am. A **21**, 2442–2446 (2004).
9. J. Yoon, S. Song, and S. Park, "Flat-top surface plasmon-polariton modes guided by double-electrode structures," Opt. Express **15**, 17151–17162 (2007).
10. D. Woolf, M. Loncar, and F. Capasso, "The forces from coupled surface plasmon polaritons in planar waveguides," Opt. Express **17**, 19996–20011 (2009).
11. M. G. Moharam, E. B. Grann, D. A. Pommet, and T. K. Gaylord, "Formulation for stable and efficient implementation of the rigorous coupled-wave analysis of binary gratings," J. Opt. Soc. Am. A **12**, 1068–1076 (1995).
12. L. Li, "Use of Fourier series in the analysis of discontinuous periodic structures," J. Opt. Soc. Am. A **13**, 1870–1876 (1996).
13. L. Li, "Formulation and comparison of two recursive matrix algorithms for modeling layered diffraction gratings," J. Opt. Soc. Am. A **13**, 1024–1035 (1996).
14. P. Lalanne and G. Morris, "Highly improved convergence of the coupled-wave method for TM polarization," J. Opt. Soc. Am. A **13**, 779–784 (1996).
15. S. Zhang and T. Tamir, "Rigorous theory of grating-assisted couplers," J. Opt. Soc. Am. A **13**, 2403–2413 (1996).
16. W. Huang, "Coupled-mode theory for optical waveguides: an overview," J. Opt. Soc. Am. A **11**, 963–983 (1994).
17. S. Olivier, M. Rattier, H. Benisty, C. Weisbuch, C. J. M. Smith, R. M. De La Rue, T. F. Krauss, U. Oesterle, and R. Houdré, "Mini-stopbands of a one-dimensional system: the channel waveguide in a two-dimensional photonic crystal," Phys. Rev. B **63**, 113311 (2001).
18. M. Åslund, J. Canning, L. Poladian, C. M. de Sterke, and A. Judge, "Antisymmetric grating coupler: Experimental results," Appl. Opt. **42**, 6578–6583 (2003).
19. W. Ding, S. R. Andrews, and S. A. Maier, "Internal excitation and superfocusing of surface plasmon polaritons on a silver-coated optical fiber tip," Phys. Rev. A **75**, 063822 (2007).
20. A. Christ, S. G. Tikhodeev, N. A. Gippius, J. Kuhl, and H. Giessen, "Waveguide-plasmon polaritons: strong coupling of photonic and electronic resonances in a metallic photonic crystal slab," Phys. Rev. Lett. **91**, 183901 (2003).
21. Z. Chen, I. R. Hooper, and J. R. Sambles, "Coupled surface plasmons on thin silver gratings," J. Opt. A, Pure Appl. Opt. **10**, 015007 (2008).
22. W. Nakagawa and Y. Fainman, "Tunable optical nanocavity based on modulation of near-field coupling between subwavelength periodic nanostructures," IEEE J. Sel. Top. Quantum Electron. **10**, 478–483 (2004).
23. R. Magnusson and Y. Ding, "MEMS tunable resonant leaky mode filters," IEEE Photon. Technol. Lett. **18**, 1479–1481 (2006).
24. H. Y. Song, S. Kim, and R. Magnusson, "Tunable guided-mode resonances in coupled gratings," Opt. Express **17**, 23544–23555 (2009).
25. W.-C. Tan, T. W. Preist, and R. J. Sambles, "Resonant tunneling of light through thin metal films via strongly localized surface plasmons," Phys. Rev. B **62**, 11134–11138 (2000).
26. D. Gérard, L. Salomon, F. de Fornel, and A. V. Zayats, "Ridge-enhanced optical transmission through a continuous metal film," Phys. Rev. B **69**, 113405 (2004).
27. Q. Cao and P. Lalanne, "Negative role of surface plasmon in the transmission of metallic gratings with very narrow slits," Phys. Rev. Lett. **88**, 057403 (2002).
28. B. Desiatov, I. Goykhman, and U. Levy, "Nanoscale mode selector in silicon waveguide for on chip nanofocusing applications," Nano Lett. **9**, 3381–3386 (2009).
29. A. Yanai and U. Levy, "The role of short and long range surface plasmons for plasmonic focusing applications," Opt. Express **17**, 14270–14280 (2009).
30. A. Sharon, D. Rosenblatt, and A. A. Friesem, "Resonant grating–waveguide structures for visible and near-infrared radiation," J. Opt. Soc. Am. A **14**, 2985–2993 (1997).